SCIENCE CHINA
Chemistry

• FEATURE ARTICLES •
• SPECIAL TOPIC • Heterogeneous catalysis theory

April 2015 Vol.58 No.4: 574–585
doi: 10.1007/s11426-015-5316-y

Surface plasmon-enhanced photochemical reactions on noble metal nanostructures

De-Yin Wu*, Meng Zhang, Liu-Bin Zhao, Yi-Fan Huang, Bin Ren* & Zhong-Qun Tian

State Key Laboratory of Physical Chemistry of Solid Surfaces; Department of Chemistry, College of Chemistry and Chemical Engineering, Collaborative Innovation Center of Chemistry for Energy Materials, Xiamen University, Xiamen 361005, China

Received October 11, 2014; accepted November 4, 2014; published online March 3, 2015

Nanoscale noble metals can exhibit excellent photochemical and photophysical properties, due to surface plasmon resonance (SPR) from specifically collective electronic excitations on these metal surfaces. The SPR effect triggers many new surface processes, including radiation and radiationless relaxations. As for the radiation process, the SPR effect causes the significant focus of light and enormous enhancement of the local surface optical electric field, as observed in surface-enhanced Raman spectroscopy (SERS) with very high detection sensitivity (to the single-molecule level). SERS is used to identify surface species and characterize molecular structures and chemical reactions. For the radiationless process, the SPR effect can generate hot carriers, such as hot electrons and hot holes, which can induce and enhance surface chemical reactions. Here, we review our recent work and related literature on surface catalytic-coupling reactions of aromatic amines and aromatic nitro compounds on nanostructured noble metal surfaces. Such reactions are a type of novel surface plasmon-enhanced chemical reaction. They could be simultaneously characterized by SERS when the SERS signals are assigned. By combining the density functional theory (DFT) calculations and SERS experimental spectra, our results indicate the possible pathways of the surface plasmon-enhanced photochemical reactions on nanostructures of noble metals. To construct a stable and sustainable system in the conversion process of the light energy to the chemical energy on nanoscale metal surfaces, it is necessary to simultaneously consider the hot electrons and the hot holes as a whole chemical reaction system.

surface plasmon resonance, plasmon-enhanced chemical reaction, *p*-aminothiophenol, density functional theory, noble metal nanostructures

1 Introduction

Decreasing size to nanoscale leads to significant changes in chemical properties and optical characters of noble metals. The nanoscale boundary effect introduces abnormal properties that are remarkably different from bulk metals. Small gold nanoparticles can exhibit excellent catalytic activity in the oxygen reduction reactions, ethene oxidation to epoxyethane, and carbon monoxide oxidation to carbon dioxide [1]. Due to the size decrease of nanoparticles [2,3], the boundary effect also leads to new optical characteristics of absorption and scattering processes. Generally speaking, surface plasmon resonance (SPR) produces strong intraband transition in the visible-light region due to the nature of free electrons in gold, silver, and copper metals [4,5]. In some studies, the surface optical electric field has been focused on specific areas that contain higher densities of energetic photons [6,7]. In addition, the photogeneration hot carriers from the relaxation of SPR may induce new channels for chemical reactions [8,9]. These special surface processes form a novel area of multidiscipline that includes surface plasmonics, surface-enhanced spectroscopy, and surface plasmon-enhanced chemical reactions [10,11]. Among surface-enhanced spectroscopies, surface-enhanced Raman spectroscopy (SERS) is a powerful surface characterization

*Corresponding authors (email: dywu@xmu.edu.cn; bren@xmu.edu.cn)

technique with a very high detection sensitivity [12,13]. SERS not only provides fingerprint information of surface species at the molecular level but also can be used to characterize the surface photochemical processes [14,15].

In this review, we introduce our recent study of surface catalytic coupling reactions of aromatic amines and aromatic nitro compounds on nanostructures of noble metals. These kinds of coupling reactions strongly depend on experimental conditions. We found that their reaction products can present very strong and characteristic SERS spectra under laser irradiation on noble metals. In Section 2, we present a brief description of the SPR and its fast relaxation processes to surface hot carriers. In Sections 3 and 4, we discuss some conflicts among results in the literature and why surface catalytic coupling reactions occurred. We also summarize the feature of SERS of aromatic azo compounds on noble metals and the enhanced chemical reactions characterized using SERS. Our proposed reaction mechanisms are given in Section 5 and our suggestions for future research in Section 6.

2 Surface plasmon resonance and its fast relaxations

Plasmon resonance of noble metals is a collective excitation of free electrons under an external field. The characteristic frequency (ω_p) of plasmon resonance of bulk metals depends on the density of free electrons, $\omega_p=(4\pi n/m_e)^{1/2}e$, where n is the density of conduction electrons, and m_e and e are effective mass and charge unit of electrons [16]. The respective plasmon resonance frequencies of bulk gold, silver, and copper metals are 9.0, 9.0, and 7.9 eV [5,16,17]. The transition energies are obviously higher than the energy of the interband transition, which inhibits the intraband transition and makes the damping constant quite large [18,19]. The relaxation time has been estimated to be approximately 10 fs.

When the size of metals decreases and the surface effect must be considered, the SPR frequency significantly redshifts to the visible light [20,21]. For silver nanoparticles, the interband channel is inhibited due to the low excitation energy [2]. In this case, the intraband transition shows some novel optical properties. The SPR effect plays an important role in light absorption and scattering processes on the nanostructures of noble metals. On the basis of the SPR effect, as shown in Figure 1(a), far-field light irradiation can be transformed to near-field photonic energy, a process that forms a sub-wavelength area or "hot spot" [22,23]. When some probing molecules are adsorbed on such a special area, they can exhibit the SERS effect or induce surface photochemical reactions [14,15,18,24]. The SPR effect can also occur on other transition metals that are similar to the noble metals (e.g., silver, gold, and copper). Nonetheless, the lifetime of SPR remains short due to either the irradiation relaxation through a photon emission or a radiationless relaxation through the generation of hot carriers [25]. Additionally, the relaxation processes are closely associated with the property of metal materials and the size of nanostructures, as well as the energy and the polarization of lasers [6a,9,11].

SPR frequency of single metal nanoparticles depends on size, shape, and the dielectric constant of environment media. As shown in Figure 1(b), when the incident photonic energy is 2.2 eV on a gold nanosphere, the lifetime of SPR is about 10 fs, which yields the photogeneration hot electrons with energy about 2.0 eV higher than the Fermi level [6a]. In this case, the hot hole was predicted to have an energy about 1.0 eV lower than the Fermi level. For a spherical silver nanoparticle with a 15 nm diameter, the SPR frequency is about 380 nm in its extinction spectrum [6a]. When the size of silver nanoparticles increases, the lifetime of hot carriers significantly decreases. For example, for a 25 nm spherical silver nanoparticle, the hot carriers mainly distribute around the Fermi level under light excitation. In contrast to smaller nanoparticles, the probability of the radiation procedure significantly increases as the size of the

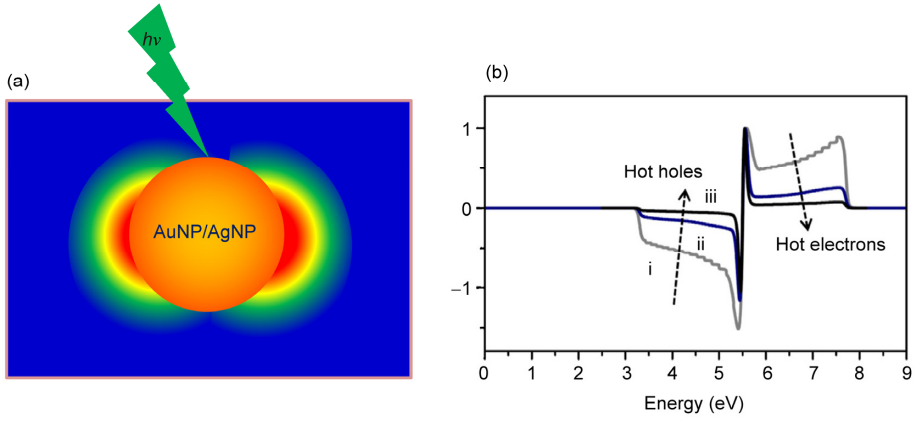

Figure 1 (a) SPR of a spherical Ag/Au nanoparticle excited by visible light; (b) normalized distribution of hot electrons and hot holes dependent on a Au slab with thicknesses of (i) 10 nm, (ii) 20 nm, and (iii) 40 nm with incident photonic energy of 2.22 eV [26].

metal nanoparticles is increased. Additionally, it was found that the distribution probabilities of high-energy hot carriers for metal nanoparticles are larger when they have longer SPR lifetimes [6a,9]. For spherical silver nanoparticles, the SPR lifetime is longer than that generated in the gold nanoparticles, due to the interband transition energy of about 2.3 eV with respect to 3.2 eV in silver nanoparticles [6a,9]. When the shape of metal nanoparticles displays as nonspherical, the polarization of laser is anisotropic; specifically, the polarization direction along the freedom within the small dimension is helpful to generate hot carriers, which in turn indicates that the distribution of photogeneration carriers is not uniform [9,26,24]. Finally, it is worthwhile to mention that for the tunneling effect of hot carriers, both high energy to overcome the energy barrier as well as large momentum perpendicular to the thin surface can be necessary [26,27]. Thus, it is possible to realize this effect in a nanocone tip with high curvity or in a small nanogap where plasmon hot spot occurs within a system of real metal nanoparticles [26,28].

3 Surface-enhanced Raman spectra of PATP

Our study of SPR enhanced chemical reactions derives from a novel idea of elucidating the enhancement mechanism in a modeling SERS system of *p*-aminothiolphenol (PATP) adsorbed on silver electrodes [11,29,30]. What follows is a brief review of SERS studies on this interesting system of PATP adsorbed on noble metal surfaces. When PATP is adsorbed on silver electrodes or nanostructures, very strong SERS signals can be easily detected [31,32]. Accordingly, PATP has been one of the most important SERS probing molecules. As shown in Figure 2(a), this is because there are some significant differences between SERS spectra and the normal Raman spectrum (NRS) of PATP, which were previously interpreted as resulting from the chemical enhancement mechanism [31,32]. The model molecule has been considered one of the most classic systems that contain a chemical enhancement mechanism in SERS fields [15]. Numerous studies have adopted the chemical enhancement mechanism to interpret their observed phenomena in SERS measurements [33,34].

SERS was first discovered from the observation of Raman spectra of pyridine adsorbed on rough silver electrodes [35–37]. SERS has been successfully extended from surface adsorptions to electrochemical reactions due to high detecting sensitivity [38,39]. The studied systems involved electrochemical reduction and oxidation reactions; for example, the reduction of nitrobenzene derivatives to corresponding aromatic amines on noble metal electrodes [38]. There has been a long history in studying the mechanism of the reduction reactions due to their importance in industry production and as intermediates for medicines and dyes. Clear evidence has been found in the disappearance of the 1338 cm^{-1} peak that corresponds to the nitro group in Raman spectra, which has demonstrated the reduction of the nitro group [40]. However, different reaction mechanisms result in difficulty when identifying surface products [41,42]. The complicated reactions, which are strongly dependent on experimental conditions, have parallel reaction pathways that form different reaction products [41,43]. On one hand, the electrochemical reduction reaction may form corresponding aromatic amines or azo compounds. On the other hand, the Raman excitation laser can induce the reduction reaction of the nitro group to corresponding aromatic amines or azo compounds when *p*-nitrobenzoic acid is adsorbed on silver films [41]. Strong debate continues on the source of observed SERS spectra on metal surfaces.

Another reason that one cannot determine surface species as aromatic amines or azo compounds has to do with the ambiguous assignment and enhancement mechanism of the SERS peaks. Previous studies investigated the SERS spectra of *p*-nitrothiophenol (PNTP) at reduced potentials on silver electrodes [32,44]. The SERS signal of the reduced product was found to be very similar to that of PATP adsorbed on a roughened silver electrode, which resulted in the proposal that the product should be PATP. However, there is a significant difference between the SERS spectra of adsorbed PATP and the solid powder of PATP. In addition, the potential-dependent SERS intensity profiles of the 1430 cm^{-1} intense peak at three excitation wavelengths of 488, 514.5, and 633 nm were observed [32]. These experimental phenomena have often been considered as the evidence of the existence of a photodriven charge transfer mechanism, as well as the charge transfer direction. For PATP-adsorbed silver electrodes, Osawa and his coworkers [32] observed that the potential corresponding to the maximum Raman peak intensity moved to a more negative potential as increasing the excitation wavelength, which indicated that the charge is transferred from the silver surface to PATP if the molecule is really adsorbed on the electrode surfaces (Figure 2(b)). Accordingly, the charge transfer mechanism has been suggested in SERS measurements of PATP adsorbed on rough silver electrodes. Numerous studies used this idea to interpret their SERS observations [15,33,34]. Additionally, some researchers think that similar SERS spectra can

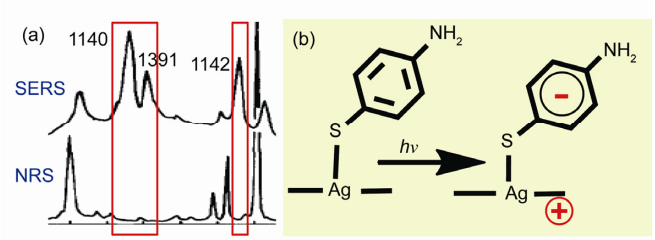

Figure 2 (a) NRS of PATP in solid states and SERS spectrum of PATP adsorbed on a roughened silver electrode with the incident laser wavelength at 514.5 nm [32]; (b) an illustration of the photo-driven charge transfer enhancement mechanism.

be observed for aromatic amines and the corresponding azo compounds on noble metal surfaces [45].

To further understand the SERS enhancement mechanism, Osawa *et al.* [32] proposed that abnormally intense SERS peaks should arise from the vibrational fundamentals with b_2 irreducible representation when PATP is considered a C_{2V} point group. The significant enhancement in SERS intensities has therefore been identified as the Herzberg-Teller vibronic coupling mechanism. The vibronic coupling occurs because the b_2 mode mediates the interaction between the charge transfer excited state and the π-π* excited state of PATP itself, located at the excitation wavelength of 300 nm [32]. The charge transfer mechanism has been widely accepted to interpret the SERS spectra of PATP adsorbed on various nanostructures of noble metals. On the basis of the charge transfer enhancement mechanism, Fromm *et al.* [33] estimated the chemical enhancement factor to be 10^7-fold when PATP was trapped at a gold bowtie nanogap. Kim and coworkers [46,47] designed different experimental measurements to support the charge transfer enhancement mechanism, including the rotation sample platform, pH effect, and ice-bath SERS experiments.

However, Hill and Wehling [31], who studied SERS of PATP adsorbed on rough silver and gold electrodes, found that the SERS signals are very sensitive to the applied potentials and the pH value of electrolyte solution. In other words, the SERS feature in acidic solutions is quite different from that in alkaline solutions. Significant differences in SERS spectra of PATP are also evident under anodic or cathodic polarization. Specially, these researchers observed better reversibility with the change of applied potentials in the SERS intensity in acidic solution than in alkaline solution. In alkaline solution, the intense SERS peaks at 1130, 1390, and 1440 cm^{-1} remain almost constant when applied potentials move negatively. To interpret this observed SERS feature, they hypothesized an isomerization of aromatic and quinonoidic configurations for PATP adsorbed on metal electrodes with applied potentials in acidic solution. To prove this assumption, the quinonoidic configuration was kept in alkaline solution even though the applied potentials were negatively moved to −1.4 V versus the Ag/AgCl reference electrode in the pure sodium disulfur electrolyte. Zhou *et al.* [34] proposed that the isomerization and the charge transfer mechanism simultaneously contributed to the SERS signal on the basis of PATP adsorbed into the nanogap between silver nanoparticles and the gold substrate.

When PATP approaches a metal surface, there are three possible adsorption configurations. Its thiol group easily binds to gold or silver surface through a strong chemical bonding, a Au–S bond, or a Ag–S bond [30]. At the same time, the S–H bond is ruptured. Other adsorption configurations arise from the amino group close to metal surfaces, where a Au–N bond or a Ag–N bond that belong to the weak coordination bond can be formed [30,48]. Finally, the thiol and amino groups may simultaneously bind to surface metal atoms. In all cases, the sulfur atom can anchor at the top, bridge, and hollow sites, all of which have large adsorption energies [30,49]. When the thiol group anchors at the top or bridge site, the adsorption configuration will have a tilted angle with respect to the surface [30]. By contrast, the molecular symmetric axis of PATP will be perpendicular to the surface at the hollow site [30,49]. According to the surface-enhanced infrared absorption spectroscopic study proposed for the self-assembled monolayer of benzenethiol on a smooth gold surface, there is a tilted angle of about 60° with respect to the surface normal. Figure 3(a) presents different adsorption configurations on rough and nanostructured surfaces that provide large probabilities for the amine nitrogen to approach surface metal atoms through the lone-paired orbital.

Figure 3(b) presents simulated Raman spectra of PATP adsorbed on different silver clusters. Some intense peaks were predicted at 379, 630, 1001, 1071, 1167, 1336, 1476, and 1596 cm^{-1}. These peak frequencies can be compared with the observed values at 379, 630, 1010, 1080, 1181, 1334, 1489, and 1588 cm^{-1} of PATP adsorbed on a roughened silver electrode in acidic aqueous solution [31]. The 1071 and 1596 cm^{-1} peaks, which are the strongest among these Raman peaks, respectively correspond to the totally symmetrically mixed vibrational modes of C–C and C–S stretchings as well as the stretching of the C–C bonds parallel to the C_2 axis [30]. The observed peaks at 1181 and 1489 cm^{-1} can be attributed to the totally symmetric C–H in-plane bending vibrations [30]. We also assumed that PATP belongs to the C_{2V} point group in free and adsorption states. Four vibrational modes with b_2 symmetry can be found in the region of 1100–1450 cm^{-1}; these were predicted at 1125, 1286, 1322, and 1426 cm^{-1} with very weak Raman intensity [49]. These b_2 modes can be closely associated with the asymmetric C–C stretching and C–H in-plane bending vibrations [49]. The vibrational analysis of free and adsorbed PATP, indicates that in this region no vibrational fundamental frequencies exist around 1390 cm^{-1}, which indicates a crucial difference between the theoretical and the experimental Raman spectra [31,32]. This result shows that the chemical enhancement mechanism cannot produce such an intense SERS peak, despite the photodriven charge transfer Herzberg-Teller vibronic coupling. To more clearly understand the vibronic coupling enhancement in the SERS spectrum of PATP, we analyzed the SERS of PATP adsorbed on silver, gold, and copper in different configurations [49]. The results caused our first doubt about the correspondence between the strong SERS peaks and the previous interpretation of the photodriven charge transfer enhancement mechanism of adsorbed PATP.

Our density functional theory (DFT) results indicated that for PATP adsorbed on noble metal surfaces, a photodriven charge transfer occurs from PATP to metal surfaces

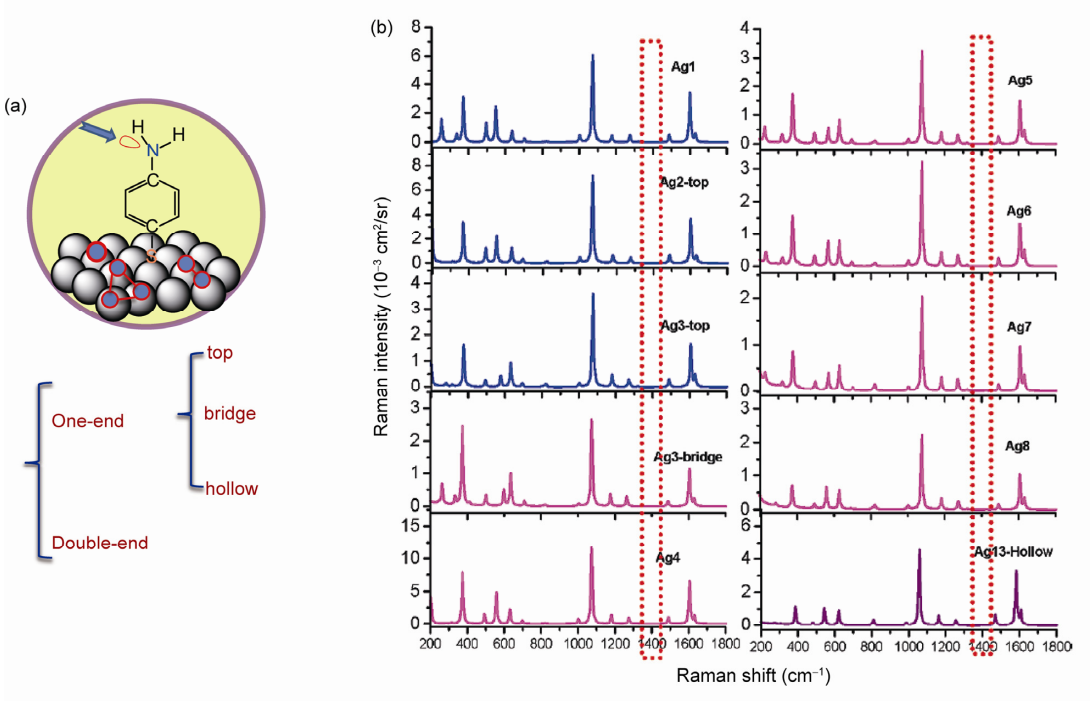

Figure 3 (a) Adsorption modeling with a one-end configuration at a top site, a bridge site, a hollow site, and with a double configuration via the interaction of the amino nitrogen binding to silver; (b) simulated Raman spectra of PATP interacting with different silver clusters. The DFT theoretical methods used are B3LYP/6-311+G** (C, N, S, and H)/LANL2DZ (Ag) from [30]. The Raman intensity was calculated based on the differential Raman scattering cross-section at the excitation wavelength of 514.5 nm. The simulated Raman spectra were expanded according to the Lorentzian lineshape with a line width of 10 cm^{-1}.

in low-lying states [50]. It is worthwhile to note that the predicted charge transfer (CT) direction contradicts that of previous studies [32,34]. We also employed a molecule-metal cluster modeling system to calculate the energies of the low-lying states. For PATP-M_n clusters (n=13), the CT transition energies were predicted at ~2.28 eV for the PATP-to-silver clusters and ~2.08 eV for the PATP-to-gold clusters [49,50]. We also checked the transition energies of the CT excited states from the M_n clusters to the PATP molecule. They were larger than 3.0 eV [49], which indicated that the CT transition energies from metal to PATP are larger than incident photonic energies in general SERS measurements. In addition, the CT energies are also larger than interband transition energies of gold and close to silver. Therefore, our DFT results indicated that the photodriven CT transition should occur in a direction from PATP to metal surfaces under visible light irradiation. In this case, the maximum potential in the potential-dependent SERS intensity profile should move positively as the laser wavelengths are increased. Although our theoretical results were in good agreement with theoretical studies from other groups [51,52], all of these predictions were opposite to the suggestions from previous studies for the SERS systems of PATP adsorbed on various metal surfaces [32,53]. This difference cast our second doubt on the SERS signal from the photodriven charge transfer enhancement mechanism of adsorbed PATP.

4 Surface catalytic coupling reactions

Except for the two points mentioned above, we noted that the charge transfer mechanism cannot be used to interpret some experimental observations. (1) For PATP adsorbed on silver or gold surfaces, the strong SERS peaks at 1140, 1390, and 1426 cm^{-1} can be observed by adopting the wide region of Raman excitation wavelengths, from 488 to 1064 nm [32,34]. For example, these strong SERS peaks can be observed in the nanogap between a silver nanoparticle and a smooth gold substrate by using an excitation wavelength of 1064 nm [34]. The UV-Vis absorption showed an absorption peak at 295 nm, which we attributed to the $\pi \rightarrow \pi^*$ transition of PATP in methanol solution that corresponded to the transition energy of about 4.20 eV. If the strong SERS peaks arise from the photodriven charge transfer state, this would contradict our prediction that the CT transition energy location would be in the range of 1.16–2.54 eV (corresponding to the incident photonic energy). Such a large energy gap between the intramolecular-excited state and the CT-excited state is inconsistent with supposition that the CT enhancement mechanism belongs to a resonance-like Raman scattering process [53–55]. (2) The pH effect on the SERS spectrum of PATP remains to be explained. Hill and Wehling [31] observed the reversibility of the SERS peak intensity ratios between 1440 and 1080 cm^{-1} with applied

potentials in the acidic solution. Although they used isomerization to interpret the reversibility, they could not interpret the occurrence of irreversibility in alkaline solution. If the strong SERS peaks are due to the charge transfer mechanism, one must still explain the relationship of the reversibility and irreversibility in terms of the pH value. These experimental observations motivated us to reconsider the possible surface species.

Accordingly, we have proposed a novel surface species for understanding these SERS phenomena. For PATP adsorbed on nanostructured metal surfaces, there are three possible reaction pathways (Figure 4(a)). The first reaction pathway (i) is the dimerization of PATP at positively applied potentials on platinum or gold electrodes in the acidic solution. In this case, PATP was oxidized to 4′-mercapto-4-aminodiphenylamine on gold and platinum electrodes [56,57]. Here, however, the simulated Raman spectrum was quite different from the SERS spectrum observed on silver electrodes [32]. The second reaction pathway (ii) is the formation of a disulfide compound from adsorbed PATP on noble metal surfaces. We noted a previous study of *p*,*p*′-diaminobenzenedisulfuride on silver films, in which the SERS spectrum of the disulfide compound on silver films was thought to have resulted from an azo compound [58]. However, it was still unclear why the surface species was formed there; additionally, the disulfide bond would be ruptured due to the strong Ag–S bond on silver surfaces [59]. The third pathway (iii) is the chemical transformation of PATP to *p*,*p*′-dimercaptoazobenzene (DMAB) due to the surface catalytic coupling reaction on noble metal surfaces. In previous studies, Yang and Fujishima *et al.* [60] suspected the existence of SERS signals from some azo compounds when SERS measurements were performed at 514.5 nm laser for PNTP self-assembled monolayer on silver films under UV illumination from a Hg-Xe lamp. They assigned the SERS peaks at 1390 and 1440 cm^{-1} to the N=N stretching vibrations and compared with the SERS spectrum of azobenzene on silver [61,62]. On the basis of our DFT calculations and our experimental results, we suggested that PATP adsorbed on noble metal surfaces can transform to DMAB adsorbed to nanostructures of silver or gold (iv) under visible laser irradiation [30,63].

Figure 4(b) presents simulated Raman spectrum (ii) of DMAB interacting with two silver clusters. For convenient comparison, Figure 4(b) presents the SERS spectra of synthesized DMAB (i) and PATP (iii) adsorbed on silver nanoparticles [63]. The simulated Raman spectrum of the DMAB complex was calculated on the basis of static polarizability derivatives [30,50]. We also obtained the simulated Raman spectra of DMAB and DMAB-Ag_n complexes through an single-end configuration that interacted with a silver cluster, but their Raman spectra were found to be very similar [30,50]. We also found that the strong Raman peaks arose mainly from the azo group and the benzene ring vibrations. This observation was also verified by experimental and theoretical studies from Sun *et al.* [64,65]. By contrast, the strong binding of the sulfur to different silver clusters was almost localized at the Ag–S bond, which slightly influenced their vibrational frequencies and the corresponding Raman intensities of these strong Raman peaks [30,50]. In the symmetric point group, the conformation of *trans* DMAB belonged to C_{2h}, which has a symmetric center; therefore, the active Raman modes belong to A_g and B_g irreducible representations.

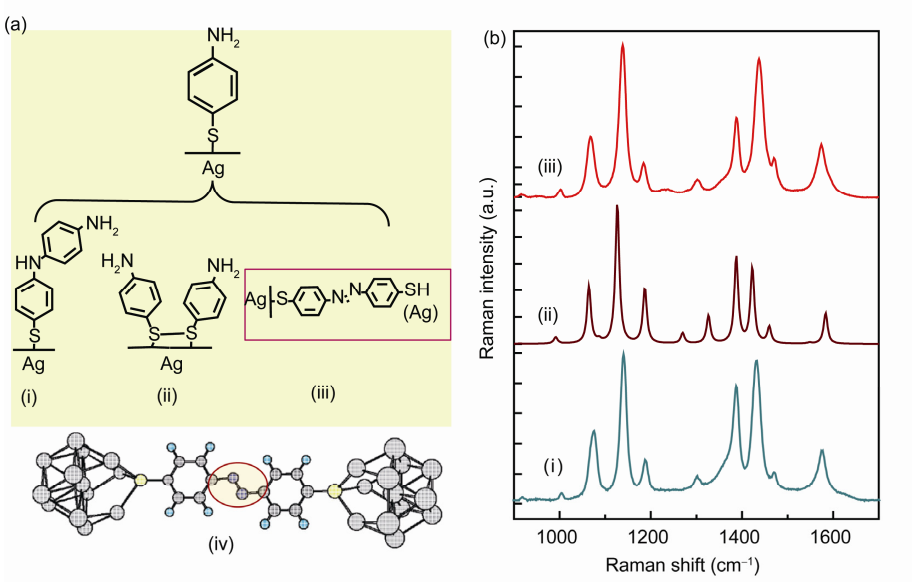

Figure 4 (a) (i–iii) Three possible reaction pathways of PATP adsorbed on nanostructured metal surfaces; (iv) displays a theoretical adsorption configuration of DMAB adsorbed on rough metal surfaces [30]. (b) Comparison of (i) observed SERS spectrum of synthesized DMAB, (ii) simulated Raman spectrum of DMAB interacting with two silver clusters at the PW91PW91/6-311+G** (C, N, S, and H)/LANL2DZ(Ag) level, and (iii) the SERS spectrum observed from PATP adsorbed on silver nanoparticles measured with the excitation line at 632.8 nm [30,63].

These results mean that the strong binding and the strong Raman peaks mainly arise from a totally symmetric vibrational mode in the azo group, as well as from the benzene ring vibrations. In terms of our vibrational analysis, these new strong Raman peaks observed at around 1130, 1390, and 1440 cm^{-1} can be attributed to the A_g totally symmetric vibrational modes [63]. The 1130 cm^{-1} peak can be assigned to the C–N symmetric stretching vibration, whereas the 1390 and 1440 cm^{-1} peaks can be assigned to the mixed vibrations of the N=N bond stretching and the C–H in-plane symmetric bending [30,63]. In our DFT calculations, we found that it is very important to choose the proper functional to predict the N=N bond distance, which is directly associated with the positions of the latter two strong peaks. When the PW91PW91 functional was combined with the triple-zeta Gaussian basis set 6-311+G**, the theoretical frequencies were in good agreement with the experimental frequencies [30,50]. If the B3LYP functional was used, however, these vibrational frequencies would be significantly overestimated. This result can be understood by comparing the calculated N=N bond length from these two methods. For example, the N=N bond distance in DMAB was optimized to 1.273 Å by PW91PW91/6-311+G** and 1.256 Å by B3LYP/6-311+G** [30]. The former is excellent compared to the experimental value of 1.260(8) Å for azobenzene measured by gas electron diffraction [66,67]. Figure 4(b) shows the theoretical spectrum (ii), which is in good agreement with experimental spectra (i) and (iii) in frequency position and Raman intensity. In contrast to DMAB, we could not obtain such a Raman spectrum from PATP adsorbed on silver even though we considered the photodriven CT mechanism. On the basis of DFT calculations, Duan *et al*. [68] also obtained good agreement with experimental SERS spectra of DMAB adsorbed on silver surfaces.

DMAB is a dye molecule with an absorption band in the visible region. The intramolecular resonance effect will contribute to the SERS measurements of DMAB adsorbed on metallic nanostructures. We found that for DMAB there exist some charge transfer states from silver to molecule in the low-lying excited states. In our previous studies we analyzed the resonance-like enhancement effect from the photodriven charge transfer mechanism and the intramolecular electronic transition [30,50]. The related molecular orbitals mainly distribute in the >C–N=N–C< azo group, which explains why the relative Raman intensities of these strong Raman peaks remained basically constant. However, these Raman peaks would become significantly stronger with the matching of photonic energies to the intramolecular resonance energy, compared with the other peaks at 1078 and 1596 cm^{-1}. Thus, the SERS signal of DMAB was easier to observe as it borrowed the surface plasmon resonance and its intramolecular resonance when PATP was oxidized to DMAB through the surface catalytic coupling reaction. On the basis of these observations, the observed SERS spectrum should belong to surface-enhanced resonance Raman spectrum of DMAB in the visible region. Moreover, these results should explain why an enormous enhancement effect can be observed in the SERS spectrum of the studied system of PATP adsorbed on silver or gold nanostructures.

The stability of DMAB depends on the acidity and applied potentials at electrochemical interfaces, which can explain the reversibility of applied potentials in acidic solution [31]. Therefore, we expected to be able to reduce DMAB to PATP in the acidic solution, which would display a good reversibility. Although the marked thermodynamic stability in the alkaline solutions maintains the structure of aromatic azo compounds, DMAB still can be reduced to PATP at very negatively applied potentials. This result demonstrates why DMAB could be reduced to PATP in acidic solution in a recent study [69].

We demonstrated that even though the abnormally strong SERS peaks arise from the surface species DMAB theoretically and experimentally, the charge transfer mechanism can still be employed to interpret the observed Raman spectra of DMAB adsorbed on silver or gold surfaces. In this case, the photodriven CT direction is from metal to DMAB. However, when PATP is adsorbed on silver or gold substrates, the photodriven charge transfer direction changes from PATP to metals under visible light. There are three points that must be re-emphasized here: (1) the fundamentals with strong Raman signals in PATP and DMAB are quite different; (2) the charge transfer directions are opposite for the low-lying excited states of PATP and DMAB adsorbed on noble metal surfaces; (3) the DMAB display of reversibility or irreversibility is strongly dependent upon the acidity of aqueous solutions. To demonstrate that the abnormal Raman peaks arise from the CT mechanism, Kim and coworkers designed numerous SERS experimental schemes, summarized as follows: (1) they continued to observe the SERS peaks at 1130, 1390, and 1430 cm^{-1} in an acidic solution with pH 3 [46]; (2) they observed that the SERS signals of the $–NO_2$ symmetric stretching gradually disappear when PNTP was adsorbed on a rotation platform with 3000 circles per minute modified with silver nanoparticles [46]. After 30 min, they could observe the strong peaks at 1130, 1390, and 1430 cm^{-1}. Because they could observe these strong peaks at once, in contrast to PNTP, they thought that PATP displayed the strong SERS peaks from PATP itself; (3) considering the temperature effect, they inferred that no photochemical reaction occurred for PATP at the boundary of ice and silver nanoparticles at liquid nitrogen temperature (77 K) because they did not observe PNTP reactions at the same boundary [70]. Even when strong reductants exist, such as $NaBH_4$, they still observed abnormally strong SERS peaks. On one hand, we thought there would be a significant difference between SERS spectra of PATP and DMAB adsorbed on noble met-

als if no reaction is occurring. On the other hand, the reaction mechanisms and their dynamics with PATP and PNTP are very different; in particular, the photochemical reaction of PATP occurs faster than PNTP. We predicted the activation energy of the rate determination step to be 5 kcal/mol for PATP and 12 kcal/mol for PNTP on silver surfaces [11,29,71]. These energy differences indicate that for PATP oxidation the reaction rate is quite fast so that one cannot detect an early photochemical reaction. Although some reports have taken this reaction mechanism into consideration, thermodynamic properties and dynamic information are lacking for such reactions. In the next section, we will introduce our thoughts about this problem and our proposed mechanisms.

5 Proposed reaction mechanisms

The reduction of aromatic nitro compounds and the oxidation of aromatic amines are classic electrochemical reactions. In 1898, Haber proposed the electroreduction mechanism for aromatic nitro compounds to aromatic amines in electrode interfaces [72]. In 2008, Corma and coworkers [73] presented selective reduction reactions from nitrobenzene to azobenzene under oxygen atmosphere on gold nanoparticles supported on TiO_2 substrates. Despite numerous studies on direct catalytic nitrobenzene reductions and aniline oxidations to azobenzene, only a few mechanistic studies have been undertaken on photochemical/ photoelectrochemical reactions on silver/gold nanostructures in the visible light region [74]. These reaction pathways are strongly dependent on experimental conditions [29,41,75]. It is known that the absorption bands of PATP and PNTP are around 300 and 326 nm, respectively, which indicate that for both molecules there is no absorption peak in the visible light region [32,76]. However, SERS spectra have shown that the respective surface reactions of PATP and PNTP can generate DMAB. These SERS results further indicated the presence of new photochemical reaction channels when the molecules are adsorbed on nanoscale silver or gold surfaces [11,29,77].

Our DFT calculations showed that charge transfer can be photoinduced from the highest occupied molecular orbital (HOMO) of PATP to the band above the Fermi level of Ag under visible light. In the general SERS process, the Raman signals can be enhanced due to the photodriven charge transfer mechanism [78]. This process is related to the radiation and radiationless relaxation processes, which correspond to the SERS effect, Rayleigh scattering, photoluminescence, induced chemical reactions, and heating. Additionally, the radiationless process can be used to estimate the rate constants of photodriven CT process based on the Fermi golden rule. In terms of theoretical calculations, the oscillator strength of the photodriven charge transfer process can be obtained by using the metallic cluster model. The metallic cluster model predicts a value of ~0.005, which indicates that the probability of the direct charge transfer transition is quite small [49,50]. Because the density of states (DOS) in silver and gold surface is uniform in visible-light region, we can assume the DOS as a constant and ρ_{0M} as the DOS value in the sp intraband. The direct CT process can be enhanced by about two orders due to the increase of the surface local optical electric field from the enhancement of the electromagnetic field.

The strong surface plasmon resonance can induce wide and strong absorption bands in the visible region. Since the lifetime of the localized SPR is about 10 fs, its radiationless relaxation generates surface hot carriers (i.e., hot electron-hole pairs). The hot electrons generated at metallic surfaces can cause reductivity. For example, the hot electrons can reduce oxygen molecules to active oxygen atoms on metal surfaces under oxygen atmosphere [71]. As shown in Figure 5(a), active oxygen species can oxidize PATP molecules adsorbed on silver nanoparticles. In this case, the amine group was oxidized to the imine group or the corresponding free radical and then dimerized to hydroazobenzene, which can be further oxidized to DMAB adsorbed on metal surfaces [11,71].

Figure 5(b) presents the hot-hole oxidization mechanism of PATP to DMAB in the absence of active oxygen species. On a metallic nanostructured surface, the lifetimes of hot electrons/hot holes were prolonged due to interfacial defects or small clusters. For PATP adsorbed on metallic surfaces, the energy of the hot hole at interfaces matched the energy position of the occupied orbital so that PATP was oxidized to a free radical cation [11,29]. In neutral or alkaline solution, the intermediate lost a proton to an imine neutral free radical, which could dimerize and further be oxidized to DMAB. The latter steps are very similar to the oxidization process by surface-active oxygen species [71]. In contrast to the direct charge transfer process, the hot-hole oxidization mechanism has a large rate constant due to the SPR effect.

The hot-hole oxidization mechanism of PATP adsorbed on nanostructured surfaces of noble metals largely depends on the experimental conditions. Numerous studies have been conducted on electron-hole generation that can induce chemical reactions in semiconductor surfaces. After the separation of electron-hole pairs, the electrons in the conduction band will participate in reduction reactions, while the holes in the valence band trigger oxidization reactions. On metal nanostructures, the energy band displays a continuum distribution around the Fermi level so that the lifetimes of the hot electrons and the hot holes obviously decrease [79]. For example, the hole lifetime is often in the range of femtoseconds on noble metal nanoparticles [19,80]. The d-band holes have longer lifetimes than excited sp-band excitation electrons of the corresponding excitation energy [81]. Few studies to date have considered the hole participating in chemical reactions on noble metal surfaces. Our results showed the relationship between the energy position

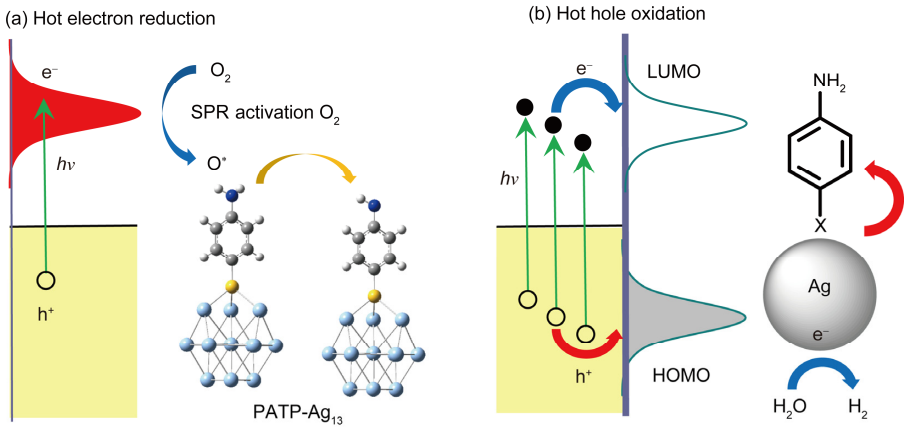

Figure 5 Oxidization mechanisms of PATP on noble metal surfaces [11]. (a) Surface oxidation coupling reaction of PATP oxidized by surface oxygen species activated by hot electrons under oxygen atmosphere in the gas/solid phase based on the PATP-Ag_{13} cluster; (b) the hot-hole oxidization mechanism in the solid/liquid interfaces. Water molecules were reduced by hot electrons to yield the hydrogen gas.

of excitation wavelengths and the pH values [11]. It is worth noting that the oxidation coupling reaction of PATP to DMAB passes through multistep processes, including electron (or hole) transfer steps and proton transfer steps. In the electrochemical SERS experiments, the chemical potentials of hot electrons, hot holes, and protons depend on applied potentials, incident photonic energy, and solution pH values [11,29]. Although the energies of hot electrons and hot holes increase with the increase of incident photonic energy, their lifetimes decrease differently with respect to the Fermi level [9,19]. The chemical potential of protons in the interfacial solution phase decreases with the pH increasing. The oxidation reaction of PATP to DMAB, which loses two electrons and two protons, favors the reaction by increasing the hot hole energy and the pH value.

6 Summary and prospects

Significant changes in photophysical as well as photochemical properties occur when molecules approach metal surfaces from gas or liquid phase. On the nanostructures of silver or gold, these changes are very interesting not only to surface-enhanced spectroscopy but also surface photocatalytic chemical reactions [6b,24,82]. We briefly reviewed our recent work on PATP oxidation and PNTP reduction on noble metal surfaces with nanoscale dimensions. We also explored the reaction mechanism of related aromatic compounds under the visible light. Because these molecules cannot yield any absorption bands in the visible light region, we thought that the photodriven charge transfer process and the interfacial chemical reaction process were related to the hot electrons and the hot holes. In the gas/solid interface, we proposed a surface catalytic coupling reaction due to the surface-activated oxygen species induced by the hot electrons. On the basis of our DFT calculations, the activation barrier on silver nanostructures is smaller than that on gold nanoparticles [11,71]. Our results explain why a PATP may cause oxidation coupling reaction very fast and with good selectivity, as well as why the surface catalytic coupling reaction was neglected in early SERS studies.

The photoreduction reaction of PNTP on silver and gold nanostructures is an obviously slower process than the photooxidation reaction of PATP. In the reduction process, the SERS signal from the symmetric stretching vibration of the nitro group gradually decreases. The dynamic change of PNTP to DMAB has been reported, but insufficient dynamic information has been provided about the photooxidation reaction for PATP adsorbed on metal surfaces. Our theoretical and experimental studies supply preliminary results for the photooxidation/photoreduction reactions. We tried to clarify the influence of different factors, including pH, laser power, incident wavelengths, and applied potentials on these reactions.

It is very attractive to consider how the enhancement mechanism of SPR may influence thermodynamic and dynamics of chemical reactions on metal nanostructures. On metal nanostructures, the SPR can enhance the local surface optical electric field to increase the probability of the charge transfer between metal and molecules. The hot electrons and hot holes produced from the SPR relaxation can participate in or induce the surface chemical reactions. Such reactions form surface transient active species, including negatively charged anions and positively charged free radicals, but do not provide dynamic information about the initial steps on metal nanostructures. In previous studies, hot electrons were widely considered in photochemical reactions on metal surfaces [83,84]. Now, it is necessary to simultaneously consider hot electrons and hot holes as a whole chemical reaction system. Thus, the metal surfaces will construct a stable and sustainable system in the conversion process of light energy to chemical energy.

After the photooxidation reaction of PATP consumes the

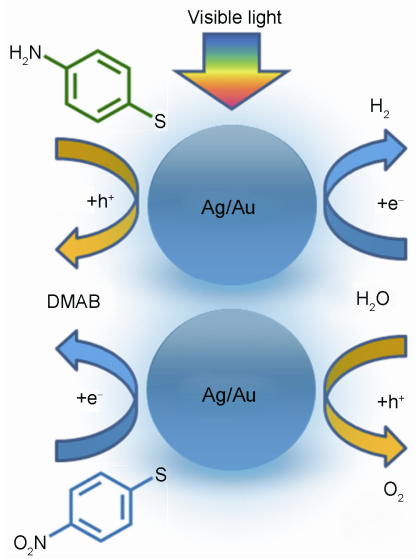

Figure 6 Utilization of surface plasmon-enhanced chemical reactions for light-splitting of water to hydrogen and oxygen. Upper: the reduction of water to hydrogen gas by the hot electrons generated from the PATP oxidation to DMAB; bottom: the oxidation of water to oxygen gas by the hot holes generated from the reduction reaction of PNTP to DMAB.

hot holes on nanostructured metal surfaces, hot electrons remain to reduce surface oxidation species. As shown at the top of Figure 6, these hot electrons can reduce hydrated protons or water molecules to hydrogen gas [85]. Additionally, the hot electrons on metal surfaces can tunnel to form hydrated electrons and then reduce the oxidation species in the solution phase. Figure 6 also presents the photoreduction reaction of PNTP to DMAB triggered by hot electrons. In this case, the hot holes may accumulate on metal surfaces to induce oxidation reactions. In aqueous solution, the hot holes can oxidize water to oxygen gas. These kinds of surface photochemical reaction take advantage of the SPR effect to convert light energies to chemical energies by inducing chemical reactions. These photochemical reactions have potential applications to promote the light energy efficiency in dye-sensitized solar cells and photocatalytic fuel cells, as well as a new perovskite solar cell.

This work was financially supported by the National Natural Science Foundation of China (21321062, 21373172). We also thank Prof. Xin Lu for his comments.

1 (a) Hutchings GJ. *Catalysis by Gold*. Singapore: Imperial College Press, 2006; (b) Parker JF, Fields-Zinna CA, Murray RW. The story of a monodisperse gold nanoparticle: $Au_{25}L_{18}$. *Accounts Chem Res*, 2010, 43: 1289–1296
2 Moskovits M. Surface-enhanced spectroscopy. *Rev Mod Phys*, 1985, 57: 783–826
3 Tian ZQ, Ren B, Wu DY. Surface-enhanced Raman scattering: from noble to transition metals and from rough surfaces to ordered nanostructures. *J Phys Chem B*, 2002, 106: 9463–9483
4 Le Ru EC, Etchegoin PG. *Principles of Surface-Enhanced Raman Spectroscopy and Related Plasmonic Effects*. Amsterdam: Elsevier, 2009
5 Johnson PR, Christy RW. Optical constants of the noble metals. *Phys Rev B*, 1972, 6: 4370–4379
6 (a) Manjavacas A, Liu JG, Kulkarni V, Nordlander P. Plasmon-induced hot carriers in metallic nanoparticles. *ACS Nano*, 2014, 8: 7630–7638; (b) Xiao M, Jiang R, Wang F, Fang C, Wang J, Yu JC. Plasmon-enhanced chemical reactions. *J Mater Chem A*, 2013, 1: 5790–5805
7 Baffou G, Quidant R. Nanoplasmonics for chemistry. *Chem Soc Rev*, 2014, 43: 3898–3910
8 Menzel D. Electronically induced surface reactions: evolution, concepts, and perspectives. *J Chem Phys*, 2012, 137: 091702
9 Govorov AO, Zhang H, Gun'ko YK. Theory of photoinjection of hot plasmonic carriers from metal nanostructures into semiconductors and surface molecules. *J Phys Chem C*, 2013, 117: 16616–16631
10 Christopher P, Xin H, Linic S. Visible-light-enhanced catalytic oxidation reactions on plasmonic silver nanostructures. *Nat Chem*, 2011, 3: 467–472
11 Zhao LB, Zhang M, Huang YF, Williams CT, Wu DY, Ren B, Tian ZQ. Theoretical study of plasmon-enhanced surface catalytic coupling reactions of aromatic amines and nitro compounds. *J Phys Chem Lett*, 2014, 5: 1259–1266
12 Tian ZQ, Ren B, Li JF, Yang ZL. Expanding generality of surface-enhanced Raman spectroscopy with borrowing SERS activity strategy. *Chem Commun*, 2007: 3514–3534
13 Wu DY, Li JF, Ren B, Tian ZQ. Electrochemical surface-enhanced Raman spectroscopy of nanostructures. *Chem Soc Rev*, 2008, 37: 1025–1041
14 Gray SK. Surface plasmon-enhanced spectroscopy and photochemistry. *Plasmonics*, 2007, 2: 143–146
15 Huang YF, Wu DY, Zhu HP, Zhao LB, Liu GK, Ren B, Tian ZQ. Surface-enhanced Raman spectroscopic study of *p*-aminothiophenol. *Phys Chem Chem Phys*, 2012, 14: 8485–8497
16 Kreibig U, Vollmer M. *Optical Properties of Metal Clusters*. Springer: Berlin, 1995
17 Ordal MA, Long LL, Bell RJ, Bell SE, Bell RR, Alexander JRW, Ward CA. Optical properties of the metals Al, Co, Cu, Au, Fe, Pb, Ni, Pd, Pt, Ag, Ti, and W in the infrared and far infrared. *Appl Optics*, 1983, 22: 1099–1120
18 Watanabe K, Menzel D, Nilius N, Freund HJ. Photochemistry on metal nanoparticles. *Chem Rev*, 2006, 106: 4301–4320
19 Chulkov EV, Borisov AG, Gauyacq JP, Sanchez-Portal D, Silkin VM, Zhukov VP, Echenique PM. Electronic excitations in metals and at metal surfaces. *Chem Rev*, 2006, 106: 4160–4206
20 Kerker M, Wang DS, Chew H. Surface enhanced Raman scattering (SERS) by molecules adsorbed at spherical particles: errata. *Appl Optics*, 1980, 19: 4159–4174
21 Pinchuk A, Kreibig U. Interface decay channel of particle surface plasmon resonance. *New J Phys*, 2003, 5: 151
22 Xu HX, Aizpurua J, Kall M, Apell P. Electromagnetic contributions to single-molecule sensitivity in surface-enhanced Raman scattering. *Phys Rev E*, 2000, 62: 4318–4324
23 Alvarez-Puebla R, Liz-Marzan LM, de Abajo FJG. Light concentration at the nanometer scale. *J Phys Chem Lett*, 2010, 1: 2428–2434
24 Ueno K, Misawa H. Surface plasmon-enhanced photochemical reactions. *J Photochem Photobio C: Photochem Rev*, 2013, 15: 31–52
25 Zhukovsky SV, Babicheva VE, Uskov AV, Protsenko IE, Lavrinenko AV. Enhanced electron photoemission by collective lattice resonances in plasmonic nanoparticle-array photodetectors and solar cells. *Plasmonics*, 2014, 9: 283–289
26 Govorov AO, Zhang H, Demir HV, Gun'ko YK. Photogeneration of hot plasmonic electrons wit metal nanocrystals: quantum description and potential applications. *Nano Today*, 2014, 9: 85–101
27 Diesing D, Kritzler G, Stermann M, Nolting D, Otto A. Metal/insulator/metal junctions for electrochemical surface science. *J Solid State Electrochem*, 2003, 7: 389–415
28 Schuck PJ. Hot electrons go through the barrier. *Nat Nanotech*, 2013, 8: 799–800
29 Zhao LB, Huang YF, Liu XM, Anema JR, Wu DY, Ren B, Tian ZQ.

A DFT study on photoinduced surface catalytic coupling reactions on nanostructured silver: selective formation of azobenzene derivatives from *para*-substituted nitrobenzene and aniline. *Phys Chem Chem Phys*, 2012, 14: 12919–12929
30 Wu DY, Liu XM, Huang YF, Ren B, Xu X, Tian ZQ. Surface catalytic coupling reaction of *p*-mercaptoaniline linking to silver nanostructures responsible for abnormal SERS enhancement: a DFT study. *J Phys Chem C*, 2009, 113: 18212–18222
31 Hill W, Wehling B. Potential-dependent and pH-dependent surface-enhanced Raman-scattering of *p*-mercaptoaniline on silver and gold substrates. *J Phys Chem*, 1993, 97: 9451–9455
32 Osawa M, Matsuda N, Yoshii K, Uchida I. Charge-transfer resonance process in surface-enhanced Raman-scattering from *p*-aminothiophenol adsorbed on silver: Herzberg-Teller contribution. *J Phys Chem*, 1994, 98: 12702–12707
33 Fromm DP, Sundaramurthy A, Kinkhabwala A, Schuck PJ, Kino GS, Moerner WE. Exploring the chemical enhancement for surface-enhanced Raman scattering with Au bowtie nanoantennas. *J Chem Phys*, 2006, 124: 061101
34 Zhou Q, Li XW, Fan Q, Zhang XX, Zheng JW. Charge transfer between metal nanoparticles interconnected with a functionalized molecule probed by surface-enhanced Raman spectroscopy. *Angew Chem Int Ed*, 2006, 45: 3970–3973
35 Fleischmann M, Hendra PJ, McQuillan AJ. Raman spectra of pyridine adsorbed at a silver electrode. *Chem Phys Lett*, 1974, 26: 163–166
36 Jeanmaire DL, Van Duyne RP. Surface Raman spectroelectrochemistry. Part I. Heterocyclic, aromatic, and aliphatic amines adsorbed on the anodized silver electrode. *J Electroanal Chem*, 1977, 84: 1–20
37 Albrecht MGC, Alan J. Anomalously intense Raman spectra of pyridine at a silver electrode. *J Am Chem Soc*, 1977, 99: 5215–5217
38 Gao P, Gosztola D, Weaver MJ. Surface-enhanced Raman-spectroscopy as a probe of electroorganic reaction pathways. 1. Processes involving adsorbed nitrobenzene, azobenzene, and related species. *J Phys Chem*, 1988, 92: 7122–7130
39 Funtikov AM, Sigalaev SK, Kazarinov VE. Surface enhanced Raman scattering and local photoemission currents on the freshly prepared surface of a silver electrode. *J Electroanal Chem*, 1987, 228: 197–218
40 Gao P, Weaver MJ. Surface-enhanced Raman-spectroscopy as a vibrational probe of electrochemical reaction-mechanisms: the electroreduction of nitrobenzene. *J Electrochem Soc*, 1987, 134: C132–C132
41 Sun S, Birke RL, Lombardi JR. Photolysis of *p*-nitrobenzoic acid on roughened silver surfaces. *J Phys Chem*, 1988, 92: 5965–5972
42 Shi C, Zhang W, Birke RL, Gosser JDK, Lombardi JR. Time-resolved SERS, cyclic voltammetry, and digital simulation of the electroreduction of *p*-nitrobenzoic acid. *J Phys Chem*, 1991, 95: 6276–6285
43 Park H, Lee SB, Kim K, Kim MS. Surface-enhanced Raman scattering of *p*-aminobenzoic acid at Ag electrode. *J Phys Chem*, 1990, 94: 7576–7580
44 Matsuda N, Yoshii K, Ataka K, Osawa M, Matsue T, Uchida I. Surface-enhanced infrared and Raman studies of electrochemical reduction of self-assembled monolayers formed from *para*-nitrohiophenol at silver. *Chem Lett*, 1992: 1385–1388
45 Kim K, Kim KL, Lee HB, Shin KS. Similarity and dissimilarity in surface-enhanced Raman scattering of 4-Aminobenzenethiol, 4,4′-dimercaptoazobenzene, and 4,4′-dimercaptohydrazobenzene on Ag. *J Phys Chem C*, 2012, 116: 11635–11642
46 Kim K, Lee HB, Shin D, Ryoo H, Lee JW, Shin KS. Surface-enhanced Raman scattering of 4-aminobenzenethiol on silver: confirmation of the origin of b_2-type bands. *J Raman Spectrosc*, 2011, 42: 2112–2118
47 Shin KS, Cho YK, Kim K. Surface-enhanced Raman scattering characteristics of 4-nitrobenzenethiol adsorbed on palladium and silver thin films. *Vib Spectrosc*, 2014, 70: 120–124
48 Zhao LB, Huang R, Bai MX, Wu DY, Tian ZQ. Effect of aromatic amine-metal interaction on surface vibrational Raman spectroscopy of adsorbed molecules investigated by density functional theory. *J Phys Chem C*, 2011, 115: 4174–4183
49 Zhao LB, Huang R, Huang YF, Wu DY, Ren B, Tian ZQ. Photon-driven charge transfer and Herzberg-Teller vibronic coupling mechanism in surface-enhanced Raman scattering of *p*-aminothiophenol adsorbed on coinage metal surfaces: a density functional theory study. *J Chem Phys*, 2011, 135: 134707
50 Wu DY, Zhao LB, Liu XM, Huang R, Huang YF, Ren B, Tian ZQ. Photon-driven charge transfer and photocatalysis of *p*-aminothiophenol in metal nanogaps: a DFT study of SERS. *Chem Commun*, 2011, 47: 2520–2522
51 Gibson JW, Johnson BR. Density-matrix calculation of surface-enhanced Raman scattering for *p*-mercaptoaniline on silver nanoshells. *J Chem Phys*, 2006, 124: 064701
52 Sun MT, Xu HX. Direct visualization of the chemical mechanism in SERRS of 4-aminothiophenol/metal complexes and metal/4-aminothiophenol/metal junctions. *ChemPhysChem*, 2009, 10: 392–399
53 Lombardi JR, Birke RL, Lu T, Xu J. Charge-transfer theory of surface enhanced Raman spectroscopy: Herzberg-Teller contributions. *J Chem Phys*, 1986, 84: 4174–4180
54 Albrecht AC. On the theory of Raman intensities. *J Chem Phys*, 1961, 34: 1476–1484
55 Kambhampati P, Child CM, Foster MC, Campion A. On the chemical mechanism of surface enhanced Raman scattering: experiment and theory. *J Chem Phys*, 1998, 108: 5013–5026
56 Hayes WA, Shannon C. Electrochemistry of surface-confined mixed monolayers of 4-aminothiophenol and thiophenol on Au. *Langmuir*, 1996, 12: 3688–3694
57 Raj CR, Kitamura F, Ohsaka T. Electrochemical and *in situ* FTIR spectroscopic investigation on the electrochemical transformation of 4-aminothiophenol on a gold electrode in neutral solution. *Langmuir*, 2001, 17: 7378–7386
58 Lu Y, Xue G. Study of surface catalytic photochemical reaction by using conventional and Fourier transform surface enhanced Raman scattering. *Appl Surf Sci*, 1998, 125: 157–162
59 Patrito EM, Cometto FP, Paredes-Olivera P. Quantum mechanical investigation of thiourea adsorption on Ag(111) considering electric field and solvent effects. *J Phys Chem B*, 2004, 108: 15755–15769
60 Yang XM, Tryk DA, Ajito K, Hashimoto K, Fujishima A. Surface-enhanced Raman scattering imaging of photopatterned self-assembled monolayers. *Langmuir*, 1996, 12: 5525–5527
61 Yang XM, Tryk DA, Hashimoto K, Fujishima A. Surface-enhanced Raman imaging (SERI) as a technique for imaging molecular monolayers with chemical selectivity under ambient conditions. *J Raman Spectrosc*, 1998, 29: 725–732
62 Yang XM, Tryk DA, Hashimoto K, Fujishima A. Examination of the photoreaction of *p*-nitrobenzoic acid on electrochemically roughened silver using surface-enhanced Raman imaging (SERI). *J Phys Chem B*, 1998, 102: 4933–4943
63 Huang YF, Zhu HP, Liu GK, Wu DY, Ren B, Tian ZQ. When the signal is not from the original molecule to be detected: chemical transformation of *para*-aminothiophenol on Ag during the SERS measurement. *J Am Chem Soc*, 2010, 132: 9244–9246
64 Fang Y, Li Y, Xu H, Sun M. Ascertaining *p,p′*-dimercaptoazobenzene produced from *p*-aminothiophenol by selective catalytic coupling reaction on silver nanoparticles. *Langmuir*, 2010, 26: 7737–7746
65 Huang Y, Fang Y, Yang Z, Sun M. Can *p,p′*-dimercaptoazobisbenzene be produced from *p*-aminothiophenol by surface photochemistry reaction in the junctions of a Ag nanoparticle-molecule-Ag (or Au) film? *J Phys Chem C*, 2010, 114: 18263–18269
66 Tsuji T, Takashima H, Takeuchi H, Egawa T, Konaka S. Molecular structure and torsional potential of *trans*-azobenzene. A gas electron diffraction study. *J Phys Chem A*, 2001, 105: 9347–9353
67 Briquet L, Vercauteren DP, Perpete EA, Jacquemin D. Is solvated *trans*-azobenzene twisted or planar? *Chem Phys Lett*, 2006, 417: 190–195

68 Duan S, Ai YJ, Hu W, Luo Y. Roles of plasmonic excitation and protonation on photoreactions of *p*-aminobenzenethiol on Ag nanoparticles. *J Phys Chem C*, 2014, 118: 6893–6902

69 Kim K, Kim K L, Shin KS. Photoreduction of 4,4′-dimercaptoazobenzene on Ag revealed by Raman scattering spectroscopy. *Langmuir*, 2013, 29: 183–190

70 Kim K, Choi JY, Shin KS. Surface-enhanced Raman scattering of 4-nitrobenzenethiol and 4-aminobenzenethiol on silver in icy environments at liquid nitrogen temperature. *J Phys Chem C*, 2014, 118: 11397–11403

71 Huang YF, Zhang M, Zhao LB, Feng JM, Wu DY, Ren B, Tian ZQ. Activation of oxygen on gold and silver nanoparticles assisted by surface plasmon resonances. *Angew Chem Int Ed*, 2014, 53: 2353–2357

72 Lund H. Cathodic reduction of nitro and related compounds. In: Lund H, Hammerich O, Eds. *Organic Electrochemistry*. 4 Ed. New York: Marcel Dekker, Inc., 2001. 379–409

73 Grirrane A, Corma A, Garcia H. Gold-catalyzed synthesis of aromatic azo compounds from anilines and nitroaromatics. *Science*, 2008, 322: 1661–1664

74 Zhu H, Ke X, Yang X, Sarina S, Liu H. Reduction of nitroaromatic compounds on supported gold nanoparticles by visible and ultraviolet light. *Angew Chem Int Ed*, 2010, 49: 9657–9661

75 Kang L, Xu P, Zhang B, Tsai H, Han X, Wang HL. Laser wavelength- and power-dependent plasmon-driven chemical reactions monitored using single particle surface enhanced Raman spectroscopy. *Chem Commun*, 2013, 49: 3389–3391

76 Kim HJ, Yoon JH, Yoon S. Photooxidative coupling of thiophenol derivatives to disulfides. *J Phys Chem A*, 2010, 114: 12010–12015

77 Sun M, Xu H. A novel application of plasmonics: plasmon-driven surface-catalyzed reactions. *Small*, 2012, 8: 2777–2786

78 Campion A, Kambhampati P. Surface-enhanced Raman scattering. *Chem Soc Rev*, 1998, 27: 241–250

79 Goldmann A, Matzdorf R, Theilmann F. Experimental hot-electron and photohole lifetimes at metal surfaces: what do we know? *Surf Sci*, 1998, 414: L932–L937

80 Zhukov VP, Aryaseitiawan F, Chulkov EV, de Gurtubay IG, Echenique PM. Corrected local-density approximation band structures, linear-response dielectric functions, and quasiparticle lifetimes in noble metals. *Phys Rev B*, 2001, 64: 195122

81 Knoesel E, Hotzel A, Wolf M. Ultrafast dynamics of hot electrons and holes in copper: excitation, energy relaxation, and transport effects. *Phys Rev B*, 1998, 57: 12812–12824

82 Brus L. Noble metal nanocrystals: plasmon electron transfer photochemistry and single-molecule Raman spectroscopy. *Accounts Chem Res*, 2008, 41: 1742–1749

83 Lindstrom CD, Zhu XY. Photoinduced electron transfer at molecule-metal interfaces. *Chem Rev*, 2006, 106: 4281–4300

84 Huang YZ, Dong B. pH dependent plasmon-driven surface-catalysis reactions of *p*,*p*′-dimercaptoazobenzene produced from *para*-aminothiophenol and 4-nitrobenzenethiol. *Sci China Chem*, 2012, 55: 2567–2572

85 Pang R, Yu LJ, Wu DY, Mao BW, Tian ZQ. Surface electron-hydronium ion-pair bound to silver and gold cathodes: a density functional theoretical study of photocatalytic hydrogen evolution reactions. *Electrochim Acta*, 2013, 101: 272–278